J Biomol NMR (2013) 57:219–235
DOI 10.1007/s10858-013-9782-2

ARTICLE

Internal protein dynamics on ps to μs timescales as studied by multi-frequency ^{15}N solid-state NMR relaxation

Tatiana Zinkevich · Veniamin Chevelkov · Bernd Reif · Kay Saalwächter · Alexey Krushelnitsky

Received: 2 June 2013 / Accepted: 6 September 2013 / Published online: 19 September 2013
© Springer Science+Business Media Dordrecht 2013

Abstract A comprehensive analysis of the dynamics of the SH3 domain of chicken alpha-spectrin is presented, based upon ^{15}N T_1 and on- and off-resonance $T_{1\rho}$ relaxation times obtained on deuterated samples with a partial back-exchange of labile protons under a variety of the experimental conditions, taking explicitly into account the dipolar order parameters calculated from ^{15}N–^{1}H dipole–dipole couplings. It is demonstrated that such a multi-frequency approach enables access to motional correlation times spanning about 6 orders of magnitude. We asses the validity of different motional models based upon orientation autocorrelation functions with a different number of motional components. We find that for many residues a "two components" model is not sufficient for a good description of the data and more complicated fitting models must be considered. We show that slow motions with correlation times on the order of 1–10 μs can be determined reliably in spite of rather low apparent amplitudes (below 1 %), and demonstrate that the distribution of the protein backbone mobility along the time scale axis is pronouncedly non-uniform and non-monotonic: two domains of fast ($\tau < 10^{-10}$ s) and intermediate (10^{-9} s $< \tau < 10^{-7}$ s) motions are separated by a gap of one order of magnitude in time with almost no motions. For slower motions ($\tau > 10^{-6}$ s) we observe a sharp $\sim$1 order of magnitude decrease of the apparent motional amplitudes. Such a distribution obviously reflects different nature of backbone motions on different time scales, where the slow end may be attributed to weakly populated "excited states." Surprisingly, our data reveal no clearly evident correlations between secondary structure of the protein and motional parameters. We also could not notice any unambiguous correlations between motions in different time scales along the protein backbone emphasizing the importance of the inter-residue interactions and the cooperative nature of protein dynamics.

Keywords SH3 domain · Solid-state · Dynamics · Relaxation · Correlation function

Electronic supplementary material The online version of this article (doi:10.1007/s10858-013-9782-2) contains supplementary material, which is available to authorized users.

T. Zinkevich · K. Saalwächter · A. Krushelnitsky (✉)
NMRGroup, Faculty of Natural Sciences II, Institut für Physik, Martin-Luther-Universität Halle-Wittenberg, Betty-Heimann-Str. 7, Saale, 06120 Halle, Germany
e-mail: krushelnitsky@physik.uni-halle.de

V. Chevelkov
Max-Planck-Institut für Biophysikalische Chemie, Göttingen, Germany

B. Reif
Department Chemie, Technische Universität München, Garching, Germany

A. Krushelnitsky
Microbiology Department, Kazan Federal University, Kazan, Russia

Introduction

NMR relaxation has proven to be one of the most powerful experimental techniques for the study of molecular dynamics in such complex molecules like proteins. Until now, it has been applied most widely to the study of protein dynamics in solution (Daragan and Mayo 1997; Dayie et al. 1996; Gaspari and Perczel 2010; Kleckner and Foster 2011; Korzhnev et al. 2001; Kroenke et al. 1998; Morin 2011; Palmer 2001). Relaxation times T_1, T_2 and NOEs, and

sometimes other relaxation parameters, measured at several resonance frequencies are usually being fitted assuming one or the other modification of the well-known "model-free" approach (Lipari and Szabo 1982a, b). Such an analysis provides the parameters of an approximate correlation function of motion which contains information on amplitude and time scale of the molecular dynamics.

Liquid-state relaxation NMR experiments are less informative for studying slow internal conformational dynamics than their solid-state analogues, since all the anisotropic magnetic interactions are averaged out by the fast isotropic Brownian tumbling of a protein as a whole (Cole and Torchia 1991). Solid-state NMR experiments of proteins potentially provide a more direct access to anisotropic and local dynamic processes on all timescales covered by NMR, however, they are subjected to methodological intricacies that caused such dynamics studies to lag behind the liquid-state mainstream. The main drawbacks of the solid-state experiments in proteins are low spectral resolution and the impossibility to use (simple) T_2 relaxation times and NOEs for molecular dynamics investigations. However, the situation changed considerably in the last decade, and now most of the methodological difficulties appear to be resolved. Up-to-date multidimensional solid-state NMR spectra of proteins provide excellent resolution (Baldus 2002; Bertini et al. 2011; Böckmann 2008; Castellani et al. 2002; Chevelkov et al. 2006; Franks et al. 2005; Marulanda et al. 2005; Zech et al. 2005), and measurements of various NMR parameters characterising internal dynamics appear at an increasing rate (Agarwal et al. 2008; Chevelkov et al. 2007, 2008, 2009a, b; Giraud et al. 2005; Krushelnitsky et al. 2009, 2010; Lewandowski et al. 2010, 2011; Mollica et al. 2012; Schanda et al. 2010, 2011; Yang et al. 2009).

In the last few years, several works employing global fits of different dynamics-sensitive solid-state NMR parameters measured on the same protein with site-specific resolution have been published (Chevelkov et al. 2007, 2009b; Lewandowski et al. 2011; Mollica et al. 2012; Schanda et al. 2010). The set of experimental parameters and the fitting functions used in these works were different. In comparison with liquid state experiments, solid-state NMR enables covering a much wider frequency range of internal dynamics and it is not yet clear which sets of data are optimal for exact and reliable determinations of the dynamic parameters, and which motional model(s) are most reasonable. In the first paper of the mentioned series (Chevelkov et al. 2009b), Reif and co-workers studied the backbone dynamics of the SH3 domain, which is also the subject of this work. They analyzed ^{15}N T_1 relaxation times at two different field strengths, ^{15}N CSA and ^{1}H-^{15}N dipole cross-correlated relaxation rates and ^{1}H-^{15}N motionally averaged dipolar couplings using a global fit for each residue. The analysis was performed using the "extended model-free approach," which assumes a two-component correlation function (Clore et al. 1990). The correlation times of these components turned out to be in the picosecond and nanosecond ranges, with a few residues showing restricted motions on the sub-microsecond time scale. Earlier, the same authors performed a combined analysis of the solution- and solid-state relaxation times T_1 and solution-NOEs in the same protein with similar results (Chevelkov et al. 2007). However, a detailed comparison demonstrated that the inclusion of the dipolar order parameters and the cross-correlated relaxation rates in the fitting does change the dynamics parameters for some residues quite appreciably.

Schanda and co-workers explored the internal molecular dynamics in ubiquitin (Schanda et al. 2010), using up to five relaxation rate constants per amide group measured at different resonance frequencies in combination with ^{1}H-^{15}N dipolar order parameters. Like in the previous paper (Chevelkov et al. 2009b), the experimental data were fitted using the "model-free" approach with a two-component correlation function and the results in general were quite similar: it was demonstrated that backbone undergoes molecular motions in the pico- and nano-second time scales, the longest slow-motion correlation time being around 300 ns.

Lewandowski et al.(Lewandowski et al. 2011) analysed site-specific ^{15}N T_1 and $T_{1\rho}$ relaxation times measured at only one resonance frequency in the GB1 protein. Since the set of the experimental parameters was rather limited, the use of a two-component correlation function was not justified. Instead, they used "wobbling in a cone" and "Gaussian axial fluctuation" and found that both models could fit the data equally well with mean correlation times around 10–20 ns. Recently, the same group of authors extended the analysis of the same protein by introducing dipolar couplings and comparing with MD simulations (Mollica et al. 2012), concluding that at least a two-component correlation function is necessary for an adequate description of the data. However, the number of the experimental parameters (namely, four: R_1's at two fields, $R_{1\rho}$ and ^{1}H-^{15}N dipolar couplings) was too small for a reliable determination of the dynamic parameters in a wide frequency range.

So far, most solid state NMR studies have used two types of data: T_1 relaxation times, which are sensitive to nanosecond molecular dynamics, and dipolar order parameters (and/or CSA-dipolar cross-correlation relaxation rate), which can provide information on low-frequency motions. There is still a gap in the time-scale region around 1 μs which was not yet sampled in solid proteins with sufficient accuracy. The most appropriate experimental tool for this purpose is a measurement of spin–lattice relaxation

times in the rotation frame (spin lock), $T_{1\rho}$. Site-specific ^{15}N $T_{1\rho}$'s have already been measured in solid proteins (Krushelnitsky et al. 2010; Lewandowski et al. 2011), however they have not been used in a global fit analysis in combination with all other available data yet except Refs. (Lewandowski et al. 2011; Mollica et al. 2012) mentioned above.

In the present work we conduct the to-date most comprehensive quantitative analysis (global fit) of a wide range of NMR data to characterize internal molecular mobility of the micro-crystalline SH3 domain of chicken alpha-spectrin. The set of the site-specific NMR parameters includes the ^{15}N spin–lattice relaxation times measured in laboratory (T_1) and rotating frames ($T_{1\rho}$) under different experimental conditions (magnetic fields, temperatures, MAS rates, on-resonance and off-resonance spin-lock frequencies) as well as the motionally averaged ^{15}N–^{1}H dipolar couplings reflecting the local dynamic order parameters. Up to now this is the most abundant set of experimental solid-state NMR dynamics-sensitive parameters measured in one protein, and we can conclude that such a multi-parameter study is imperative to arrive at valid conclusions on the internal protein dynamics. These experimental data taken together enable a robust analysis of molecular dynamics in a correlation time range of about 6 orders of magnitude. Taking into account the dipolar CODEX study of slow motions in the same protein which is "model-free" and does not rely on multi-parameter fitting (Krushelnitsky et al. 2009), modern solid-state NMR techniques now cover a time range of 9–10 orders of magnitude.

We stress that all experiments have been performed on the deuterated SH3 samples with a partial back-exchange of labile protons, using proton detection of a signal (Chevelkov et al. 2006). Deuteration is absolutely necessary for this kind of work for three reasons: first, proton detection enhances the sensitivity, which enables performing a large number of experiments within reasonable time limits; second, proton dilution significantly reduces the proton-driven spin diffusion between ^{15}N nuclei, and we claim that distortions of the ^{15}N relaxation rates by the spin-diffusion effect are negligible; third, highly deuterated proteins provide highest resolution without any high power decoupling enabling using rather long RF spin-locks. The suppression of the spin diffusion and proton detection can be also achieved using high MAS rates even in fully protonated proteins (Lewandowski et al. 2011; Lewandowski et al. 2010), however, the proton line width is in this case still not as small as for deuterated proteins. Even more importantly, high MAS rates make studying the detailed spin-lock dependencies of $T_{1\rho}$ relaxation times more difficult (see the details below), which renders $T_{1\rho}$ less sensitive to slow dynamics.

The analysis of the NMR data has been conducted using a "model-free" approach assuming the presence of one up to three distinguishable motional processes in order to find a reasonable compromise between a good fit of the data and a minimum number of fitting parameters. In addition to the discrete components of the composite correlation function, we also tested a smooth distribution of the correlation times for the slow-motion region, which may reflect its complex nature. The analysis has provided us with detailed quantitative data on the internal protein dynamics and allowed making new and relevant conclusions on the nature of internal protein mobility over a wide range of correlation times.

Experimental data

In this work we analysed the solid state NMR data measured in previous experimental studies of the SH3 domain. Most of them were published, and some of them were measured but not published explicitly. Below is the list of the experimental NMR parameters used in our analyses:

- ^{15}N–^{1}H motionally averaged dipolar couplings (order parameters) measured at 400 MHz (^{1}H resonance frequency), MAS rate 20 kHz, t = 11 °C (Chevelkov et al. 2009a);
- ^{15}N T_1 at 400 MHz, MAS rate 13 kHz, t = 12 °C (Chevelkov et al. 2008);
- ^{15}N T_1 at 600 MHz, MAS rate 13 kHz, t = 12 °C (Chevelkov et al. 2008);
- ^{15}N T_1 at 900 MHz, MAS rate 13 kHz, t = 12 °C (Chevelkov et al. 2008);
- ^{15}N T_1 at 600 MHz, MAS rate 10 kHz, t = 14 °C (Krushelnitsky et al. 2009);
- ^{15}N T_1 at 600 MHz, MAS rate 10 kHz, t = 24 °C (Krushelnitsky et al. 2009);
- ^{15}N $T_{1\rho}$ at 400 MHz, MAS rate 20 kHz, on-resonance spin-lock 8 kHz (^{15}N resonance frequency in the rotating frame), t = 10 °C (Krushelnitsky et al. 2010);
- ^{15}N $T_{1\rho}$ at 400 MHz, MAS rate 20 kHz, on-resonance spin-lock 13 kHz, t = 27 °C (Krushelnitsky et al. 2010);
- ^{15}N $T_{1\rho}$ at 400 MHz, MAS rate 20 kHz, on-resonance spin-lock 8 kHz, t = 27 °C (Krushelnitsky et al. 2010);
- ^{15}N $T_{1\rho}$ at 600 MHz, MAS rate 10 kHz, off-resonance spin-lock 35 kHz (effective ^{15}N resonance frequency in the tilted rotating frame), the off-resonance angle between B_0 and B_{1e} fields 24°, t = 14 °C (Krushelnitsky et al. 2010);
- ^{15}N $T_{1\rho}$ at 600 MHz, MAS rate 10 kHz, off-resonance spin-lock 35 kHz, off-resonance angle 24°, t = 24 °C (Krushelnitsky et al. 2010);

- ^{15}N $T_{1\rho}$ at 600 MHz, MAS rate 10 kHz, off-resonance spin-lock 46.3 kHz, off-resonance angle 24°, t = 14 °C (Krushelnitsky et al. 2010).

For some residues not all the data mentioned above were available. The T_1 relaxation decays measured in (Krushelnitsky et al. 2009) were used for the normalisation of the dipolar CODEX decays and thus the relaxation delays in these experiments did not exceed the mixing times in these experiments (about 3–4 s). Thus, long relaxation times (longer than $T_1 \sim$ 20–50 s depending on the peak intensity) could not be determined accurately and were excluded from the analysis. A similar problem occurred with the off-resonance $T_{1\rho}$ measurements: the maximum duration of the spin-lock pulse was limited to 100–150 ms to avoid sample heating and transmitter damage. Hence, relaxation times longer than 1–4 s (again, depending on the peak intensity) could not be measured with the acceptable accuracy (on-resonance $T_{1\rho}$'s were much shorter and 100 ms spin-lock pulses were always sufficient for the determination of the relaxation times). The details of all the experiments are presented in the corresponding references. A table containing all the experimental data used in the fitting for each residue is presented in the Supplementary material.

In total 54 peaks in 2D ^{15}N–^{1}H correlation spectrum corresponding to backbone amides and 8 peaks corresponding to the side chain ^{15}N atoms could be resolved (the SH3 domain has 62 residues in total). Two pairs of residues (K18 and K59, E17 and E22) cannot be resolved because of signal overlap. Thus, the dynamic parameters obtained for these two pairs must be considered average values.

Data analysis

The analysis described below aims at a determination of the various parameters in the correlation function of motion from the relaxation data. The correlation function contains quantitative information about the amplitudes and correlation times of the ^{15}N–^{1}H vector reorientation, which is the ultimate goal of the data treatment. In the following, we discuss the theoretical framework used in our analyses.

Theoretical description of R_1 and $R_{1\rho}$

There are two main mechanisms responsible for the ^{15}N relaxation: ^{15}N–^{1}H dipolar coupling and ^{15}N chemical shift anisotropy (CSA) tensor reorientation. In our recent work (Kurbanov et al. 2011) we have derived general $R_1/R_{1\rho}$ formulas for these two relaxation mechanisms. These formulae are valid for arbitrary values of the off-resonance angle of the spin-lock field as well as spin-lock and MAS frequencies (except the rotary resonance condition). We stress the use of off-resonance spin lock irradiation to increase the effective frequency without running into transmitter issues or sample heating problems. For the dipolar relaxation mechanism between two nuclei with spins S and I the relaxation rate under RF spin-lock can be expressed as

$$R_{1\rho}^{IS} = R_1^{IS} + \sin^2\theta_\rho\left(R_{1\Delta}^{IS} - \frac{1}{2}R_1^{IS}\right); \quad (1)$$

where

$$R_1^{IS} = \mu_S^2(J_0(\omega_I - \omega_S) + 3J_1(\omega_I) + 6J_2(\omega_I + \omega_S)); \quad (2)$$

$$R_{1\Delta}^{IS} = \mu_S^2\left(3J_1(\omega_S) + \frac{1}{3}J_0(\omega_e - 2\omega_R) + \frac{2}{3}J_0(\omega_e - \omega_R) + \frac{2}{3}J_0(\omega_e + \omega_R) + \frac{1}{3}J_0(\omega_e + 2\omega_R)\right); \quad (3)$$

The dipole–dipole coupling constant reads $\mu_S = \frac{\hbar\gamma_I\gamma_S}{r^3}\sqrt{\frac{S(S+1)}{3}}$ depends on the internuclear distance r and the gyromagnetic ratios γ_I and γ_S, $\hbar$ is the Planck's constant; $J_{0,1,2}(\omega)$ is the spectral density function of the order 0,1,2; ω_e is the effective spin-lock circular frequency; ω_I and ω_S are the circular resonance frequencies of I and S nuclei, respectively; ω_R is the MAS frequency in rad/s; θ_ρ is the off-resonance angle between the external magnetic field B_0 and the applied RF field B_{1e} fields. If $\theta_\rho = 0°$ or 90°, then Eq. (1) transforms to the standard R_1 and $R_{1\rho}$ formulas for the heteronuclear dipolar relaxation mechanism, respectively.

In close analogy, the relaxation rate expressions for the CSA mechanism can be written as

$$R_{1\rho}^{CSA} = R_1^{CSA} + \sin^2\theta_\rho\left(R_{1\Delta}^{CSA} - \frac{1}{2}R_1^{CSA}\right); \quad (4)$$

where

$$R_1^{CSA} = \frac{3}{4}(\delta\omega_I)^2 J_1(\eta, \omega_I); \quad (5)$$

$$R_{1\Delta}^{CSA} = \frac{1}{6}(\delta\omega_I)^2\left(\frac{1}{2}J_0(\eta, \omega_e - 2\omega_R) + J_0(\eta, \omega_e - \omega_R) + J_0(\eta, \omega_e + \omega_R) + \frac{1}{2}J_0(\eta, \omega_e + 2\omega_R)\right). \quad (6)$$

Here, δ is the reduced anisotropy $\delta = \delta_{zz} - \frac{1}{3}(\delta_{xx} + \delta_{yy} + \delta_{zz})$ in ppm units; η is the shielding asymmetry $\eta = \frac{\delta_{xx} - \delta_{yy}}{\delta}$. The explicit expression for the spectral density function $J(\eta, \omega)$ for the general case can be found in (Kurbanov et al. 2011), however in our analysis we assume the CSA tensor of ^{15}N in a protein to be axially symmetric and hence $\eta = 0$. In this case the spectral density functions in Eqs. (1) and (4) are the same. We also

assume that the ^{15}N–^{1}H bond and the main axis of the CSA tensor coincide which is true in the first approximation: the angle between ^{15}N–^{1}H bond and the main CSA tensor axis is about 20° for backbone (Chekmenev et al. 2004) and about 30° for the side chain ^{15}N atoms (Herzfeld et al. 1987). However, this may affect the analysis only in the case of very specific and also improbable motional models that may cause different reorientation amplitudes experienced by the interatomic bond and the CSA tensor. Thus, the experimentally observed relaxation rate is

$$R_{1\rho} = R_{1\rho}^{IS} + R_{1\rho}^{CSA}, \tag{7}$$

and the assumptions mentioned above enable us using the same spectral density functions in calculating both dipolar and CSA contributions to the relaxation rate. The anisotropy δ was assumed to be 160 ppm (Chekmenev et al. 2004; Hall and Fushman 2006; Wylie et al. 2006, 2007). The ^{15}N–^{1}H bond length used for calculation of the order parameter was set to 1.015 Å (Yao et al. 2008), which corresponds to a ^{15}N–^{1}H dipolar coupling 11.64 kHz. The spectral density functions $J_0(\omega)$, $J_1(\omega)$ and $J_2(\omega)$ for isotropic samples are equal, which was demonstrated on the "wobbling in a cone" model simulations (Kurbanov et al. 2011), and the indexes 0, 1, and 2 further will be omitted.

It is worthwhile mentioning the issue of the interfering coherent spin–spin contribution to the $R_{1\rho}$ relaxation rate that emerges due to the additional relaxation pathway through the proton dipolar reservoir (Akasaka 1983; Krushelnitsky et al. 2002; Lewandowski et al. 2011; Vander-Hart and Garroway 1979). Care must be taken in order to either take this contribution into account or make it negligible. In our case we suppress this contribution by use of a deuterated sample in which the proton density is rather low and thus the proton dipolar reservoir becomes negligible. Lewandowski and colleagues (Lewandowski et al. 2011) have demonstrated that at MAS rates around 60 kHz the spin–spin contribution should be negligible even in a fully protonated protein. The proton linewidth (which is a direct measure of the ^{1}H-^{1}H coupling and hence, the efficiency of the spin–spin contribution) in a fully protonated protein at 60 kHz MAS is 150–200 Hz (Marchetti et al. 2012) whereas in the deuterated protein at 10–20 kHz spinning we have a proton linewidth of merely 20–30 Hz (Chevelkov et al. 2006), i.e., almost one order of magnitude less. Thus, we conclude that with the deuterated protein, we are well on the safe side in neglecting this contribution in the analysis.

Correlation functions and spectral densities

Our analysis follows the spirit of the "model-free" approach (Lipari and Szabo 1982a, b) that divides the normalized correlation function into two parts—non-averaged (order parameter S^2) and time-dependent $(1 - S^2)$ contributions to the reorientation autocorrelation function. $(1 - S^2)$ represents a dimensionless amplitude of motion. In the case of several independent motional processes, the correlation function can be written as

$$C(t) = \prod_{i=1}^{N_m} \left[S_i^2 + (1 - S_i^2) \cdot \exp(-t/\tau_i)\right], \tag{8}$$

where N_m is a number of motional processes, S_i^2 and τ_i are order parameter and the correlation time of the ith process.

For exponential loss of correlation, the spectral density function for a single motional process at $\omega > 0$ can be expressed as

$$J(\omega) = \left(1 - S^2\right) \frac{\tau}{1 + (\omega\tau)^2}. \tag{9}$$

Since the relaxation measurements were conducted at different temperatures, we take into account the temperature dependence of the correlation times. We assume Arrhenius dependence,

$$\tau(T) = \tau_{293K} \exp\left(E_a/R\left(\frac{1}{T} - \frac{1}{293K}\right)\right), \tag{10}$$

where E_a is the activation energy, R—universal gas constant, τ_{293K} is the correlation time at 293 K.

The main reason we are analyzing the data measured at different temperatures is that simply considering the correct sign of the slope of the temperature dependence of the relaxation rates enables a more exact determination of the correlation times of motions. We stress that even though our temperature range is narrow, the fact that the fitted apparent activation energies in most cases have the correct sign demonstrates internal consistency in that the dependence of the dynamics on temperature is indeed reflected in the data with statistical relevance. Thus, sacrificing the temperature dependences would make the fitting less certain, in spite of the additional assumption we need to make. In the analysis we assume the order parameters to be temperature-independent which is strictly speaking not true. However, introducing a temperature dependence in the fitting model may appear unreasonable at this point since it is associated with increasing the number of fitting parameters and thus, the uncertainty of the fitting results. A liquid-state NMR studies of the temperature dependences of the order parameters (Chang and Tjandra 2005; Johnson et al. 2007) demonstrate that these dependences are rather strong at temperatures above 35 °C, and within the range from 12 to 27 °C (the limiting temperatures of our experiments), the S^2 variation is just slightly above the experimental error. Solid state NMR measurements of the ^{1}H-^{15}N dipolar coupling in amorphous lyophilized rehydrated

protein powders (Hackel et al. 2012) show no experimentally detectable difference between 10 and 25 °C at all. Thus, we conclude that neglecting the temperature dependence of the order parameters within the narrow temperature range does not cause any essential error in the fitting.

For the case of two motional modes the spectral density function has a form

$$J(\omega) = \left(1 - S_2^2\right) \frac{\tau_2}{1 + (\omega\tau_2)^2} + S_2^2\left(1 - S_1^2\right) \frac{\tau_1}{1 + (\omega\tau_1)^2}, \tag{11}$$

where τ_1 and τ_2 are the correlation times of the slow and fast motions, respectively. The maximum number of motions that we used in our analysis is three. Assuming that the correlation times of these motions obey the condition $\tau_3 \ll \tau_2 \ll \tau_1$ then the corresponding density function is

$$J(\omega) = S_3^2\left[\left(1 - S_2^2\right) \frac{\tau_2}{1 + (\omega\tau_2)^2} + S_2^2\left(1 - S_1^2\right) \frac{\tau_1}{1 + (\omega\tau_1)^2}\right] + \left(1 - S_3^2\right) \frac{\tau_3}{1 + (\omega\tau_3)^2}. \tag{12}$$

If the third motion is rather fast obeying $\tau_3 \ll \omega^{-1}$, then the last term in Eq. (12) is negligible in comparison with the first one and the spectral density can be simplified to

$$J(\omega) = S_3^2\left[\left(1 - S_2^2\right) \frac{\tau_2}{1 + (\omega\tau_2)^2} + S_2^2\left(1 - S_1^2\right) \frac{\tau_1}{1 + (\omega\tau_1)^2}\right]. \tag{13}$$

The dipolar order parameter must be equal to

$$S_{\text{exp}}^2 = S_1^2 \cdot S_2^2 \cdot S_3^2. \tag{14}$$

S_{exp} was determined as the ratio of the experimental ^{15}N–^{1}H dipolar coupling constant to the rigid-lattice value (11.64 kHz). It should be mentioned that Eq. (14) assumes that the correlation times of all three motions are shorter than a few microseconds, since the slower motions do not contribute to the motional averaging of the dipolar coupling (Chevelkov et al. 2009a). Our results, however, demonstrate that some residues undergo motions with the correlation times around 10^{-5} s (see below) which invalidates Eq. (14). Yet, as will be shown below, the amplitude of such slow motions is much smaller than the experimental error of the dipolar coupling measurements. Thus, this problem may safely be neglected. We here note that an experimental error in S_{exp} in the range of a few percent is not in contradiction with the much more accurate extraction of values for $(1 - S^2)$ in the sub-percent range from the joint fit of relaxation data (see below), in which the larger error margin of S_{exp} is taken into account.

Equations (8) and (9) assume that the correlation function of a separate motional process is single-exponential. However, even for relatively simple motional models the correlation function has a more complex shape. In addition, there can be a distribution of correlation times, i.e., the sample may exhibit dynamic inhomogeneities. To check if the non-exponentiality of the correlation function may affect the results of the data analysis, in some cases we used the Fuoss-Kirkwood distribution function (Beckmann 1988). In this case the spectral density function has a similarly compact form

$$J(\omega) = \frac{\beta}{\omega} \cdot \frac{(\omega\tau)^{\beta}}{1 + (\omega\tau)^{2\beta}}, \tag{15}$$

where β $(0 < \beta < 1)$ is the distribution width parameter. The cases $\beta = 1$ and $\beta = 0$ correspond to infinitely narrow (delta-function) and infinitely wide distributions, respectively. Although the Fuoss-Kirkwood distribution is a phenomenological function, it successfully describes actual NMR and dielectric data in synthetic polymers (Fedotov and Schneider 1989) quite well. In the Supplementary material we present the comparison of the correlation functions for the "wobbling-in-a-cone" model inferred from computer simulations and a numerical integration of the correlation function using the Fuoss-Kirkwood distribution function (Fig. S1). As it is seen, the correspondence between the two types of the correlation functions is rather good for all cone angles. It should also be mentioned that the description of the "wobbling-in-a-cone" model with the help of the distribution function demonstrates that the assumption on the single-exponential form of the correlation function, see Eq. (8), is seriously violated only for large-amplitude diffusive motions, otherwise, the assumption seems to be quite reasonable.

We close this section with the general remark that the potential complexity of internal protein dynamics is as yet not fully acknowledged in the common models used to describe NMR relaxation properties. In the synthetic polymer community, strongly non-exponential correlation functions are the rule rather than the exception, simply arising from the presence of different modes in a complex, coupled system (Doi and Edwards 1986). Such mode distributions commonly lead to orientation correlation functions that exhibit a power law over a certain time range, which can well be modeled by the mentioned Fuoss-Kirkwook spectral density function. This and many others, such the Cole-Davidson, Cole-Cole, and Havriliak-Negami functions, are commonly used in dielectric, mechanical or NMR relaxation studies of polymers (Ferry 1980; Kremer and Schonhals 2003; McCrum et al. 1967). The fact that protein dynamics can be described by very similar theoretical models (Haliloglu et al. 1997) stresses the necessity

of critically evaluating such potentially more realistic fitting models.

Fitting strategy and error considerations

The experimentally determined relaxation rates and dipolar order parameters can be described by a set of fitting parameters which includes order parameters, correlation times at 293 K, activation energies and (if used) the distribution width parameters for each motion. These parameters were defined from simultaneous fitting all available relaxation rates and dipolar couplings for each residue. Fitting aimed to minimize the following expression

$$\chi = \sqrt{\frac{1}{N+1}\left(\sum_{i=1}^{N}\left(\frac{T^i_{\exp}-T^i_{sim}}{\delta T^i_{\exp}}\right)^2+\left(\frac{S^2_{\exp}-S^2_1\cdot S^2_2\cdot S^2_3}{\delta S^2_{\exp}}\right)^2\right)}, \quad (16)$$

where T^i_{sim} and $T^i_{\exp}$ are the calculated (using the fitting parameters) and experimental relaxation times, respectively, N is a number of experimentally available relaxation times, $\delta T^i_{\exp}$ and $\delta S^2_{\exp}$ are the experimental errors of the relaxation times and dipolar order parameters, respectively. The minimization procedure was performed with a Monte-Carlo algorithm. Each minimization consisted of 10^6 steps. The mean values of the fitting parameters as well as their root mean square deviations were obtained from the Monte-Carlo trajectories.

Because of the narrow temperature range of the experiments, the uncertainties for the activation energies E_a were rather high. In some cases, E_a's were unreasonably high or low. The activation energies have only a minor impact on the other dynamic parameters, thus paying attention to the E_a values is hardly worthwhile. At the same time, the fitting quality χ depends on the activation energies quite appreciably. Since we will be comparing the fitting errors for different fitting models (see below) we used the following procedure of the fitting. First, we fitted the data for all the residues without any limitations. Then we excluded the E_a values below 10 and above 100 kJ/mole as physically unreasonable. For the rest of the values we calculated the mean E_a and root-mean-square deviation. Then we run the Monte-Carlo simulations again limiting the E_a's within mean value ± RMSD. The table of the activation energy limits during the Monte-Carlo simulations for each fitting model is shown in the Supplementary material (Table S2). We stress again that the simple fact that positive values are obtained proves the statistical significance of implementing a temperature dependence, rather than just treating the experiments at different but close temperature as repeated measurements. In addition, if the fitting model assumes two activation energies, then the activation energy of the slow motion during the Monte-Carlo trajectory at each step cannot be lower than that of the fast motion. As mentioned above, such limitations of the activation energies have rather small influence on the order parameters and correlation times.

Results and discussions

Data analysis using different fitting models

The first step in the data analysis is a choice of the model of the motional correlation function and set of the dynamic fitting parameters. Proteins undergo a complex hierarchy of internal motions in an extremely wide timescale range. Thus, fitting the data assuming only one mode of motion is an evident oversimplification (Mollica et al. 2012; Schanda et al. 2010). On the other hand, using unreasonably complicated models and large number of the fitting parameters may lead to a meaningless over-interpretation. For the comparison of different options, we performed the data fitting using four different motional models starting from the simplest model and then sequentially increasing the number of motions and fitting parameters. The abundant set of data allowed us to test more complicated models in comparison to what has been done in previous studies.

The simplest model assumes only one single-exponential component of the correlation function and the spectral density function in the form of Eq. (9). This model will be referred as "one component" model. This model has only three fitting parameters: the order parameter S^2, a correlation time τ and the activation energy E_a. As expected, the fitting quality of the data is the worst out of all models (Fig. 1a). Note the systematic inconsistency between the experimental (objective) and the fitted order parameters (Fig. 1b), which represents a good criterion that this model is physically unreasonable.

The next step is the "two components" model. It assumes two discrete exponential components of the correlation function and the spectral density function in the form of Eq. (11). This model correspondingly requires six fitting parameters: an order parameter, correlation time and activation energy for each mode. Not surprisingly, the fitting quality improves significantly, see Figs. 1 and 2. There is only one residue, Q50, for which the introduction of additional motion did not improve the fitting error; all other residues reveal an appreciable decrease of χ upon introduction of the second motion.

The same conclusion on the significant improvement of the fitting quality upon transition from "one component" to "two components" models was made by Schanda et al. (2010). It is, however, interesting to note that while fitting the data using the "one component" model, they obtained

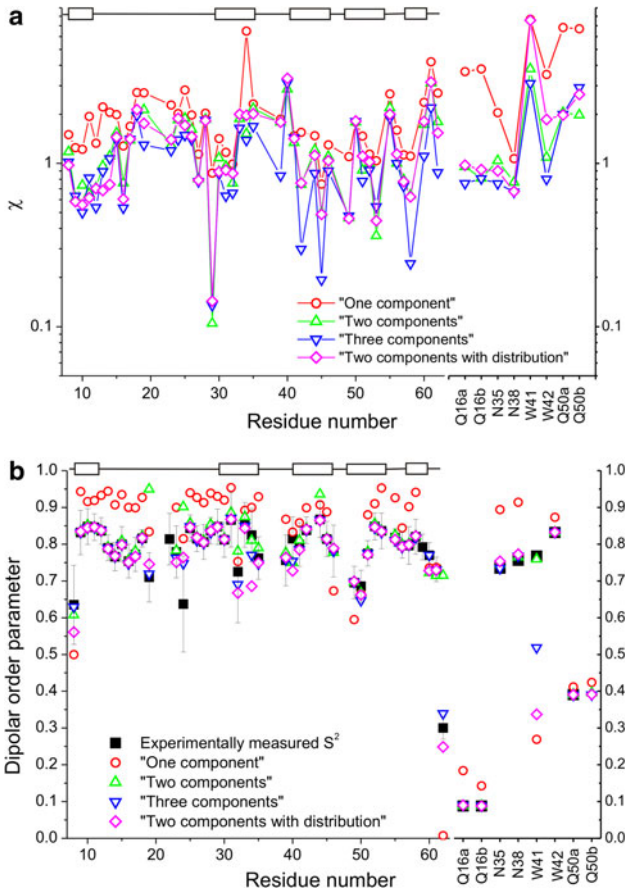

Fig. 1 **a** χ (Eq. 16) and **b** dipolar experimental and calculated order parameters as a function of residue number for different fitting models. The *right hand sides* of the plots correspond to the side chains resonances. β-sheets are depicted on the *top* of the plots (SH3 domain has no helices)

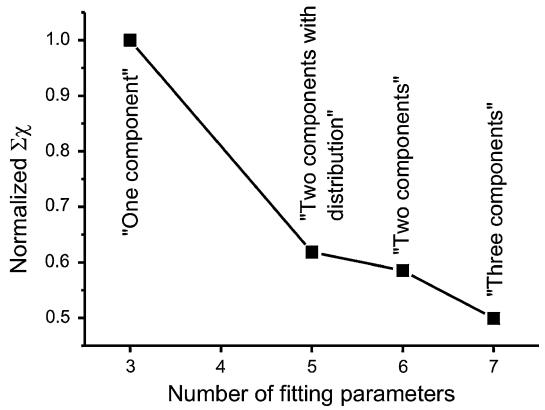

Fig. 2 Summed χ over all residues normalized to the "one component" model for different fitting models

the information on the fast motion on the ps time scale. In contrast, our "one component" model gives correlation times in the ns range (Fig. S2). Obviously, this is due to the $T_{1\rho}$ data, which were used in our analysis and were absent in the analysis of Schanda et al. This finding is in good correspondence with the "one component" fitting performed in (Lewandowski et al. 2011; Mollica et al. 2012): the analysis of the T_1 and $T_{1\rho}$ relaxation times also provides the correlation time of motion in the ns range. Since $T_{1\rho}$ data are sensitive to slower motions, including them in the analysis shifts the correlation time towards slower (larger) values. All this clearly indicates that analyzing a limited set of experimental data using a simplified model may provide good fitting quality but physically meaningless results.

In addition to these models we checked two more complicated options of the analysis. One of them is a model of three discrete motions ("three components" model). The number of the fitting parameters in this case must be nine, however we reduced this number to seven assuming the fastest motion to be too fast: if the correlation time of this motion is shorter than $\sim 10^{-11}$ s, then the spectral density function for this model has the form given by Eq. (13). Thus, the correlation time and the activation energy of the fast motion cannot be determined from the fitting, and the number of the fitting parameters for this model is seven: order parameters, correlation times and activation energies for the slow and intermediate motions and the order parameter for the fast motion. As one may see from Fig. 2, introducing the third motion improves the overall fitting quality, although not too much. At the same time, for some residues the fitting improvement is quite significant, see Fig. 1a.

Finally, we checked one more model ("two components with distribution") which includes two motions: the fast motion is assumed to be very fast (correlation time $<10^{-11}$ s) and the second motion has a smooth distribution of the correlation times. Unlike fast dynamics, slow internal dynamics in proteins are associated with overcoming high energy barriers which is only possible if different conformational degrees of freedom take part in this motion. Slow motions involve a complex network of intra-protein interactions (Haliloglu et al. 1997) and hence, the correlation function of motion can be quite complicated. Thus, the assumption on the distribution of the correlation times may be quite reasonable. This model has five fitting parameters: the order parameter for the fast motion and the order parameter, correlation time, activation energy and distribution width parameter for the slow motion. The spectral density function is then a combination of Eq. (11)—assuming $\tau_f < 10^{-11}$ s—and Eq. (15):

$$J(\omega) = S_f^2 \left[\left(1 - S_S^2\right) \frac{\beta}{\omega} \frac{(\omega\tau_S)^{\beta}}{1 + (\omega\tau_S)^{2\beta}} \right]. \quad (17)$$

In general, this model provides approximately the same fitting quality as the "two components" model (see Fig. 2). Trying other more complicated models is of course possible but even with the present most comprehensive

(up to date) dataset this would hardly be physically justified.

While comparing different models, one should consider not only the fitting errors, but also the number of fitting parameters: the simpler the model, the better. Quantitative compromise between the fitting error and the number of the fitting parameters can be determined using the Akaike Information Criterion (*AIC*) (Akaike 1974) which takes penalties not only for the fitting error but also for the number of fitting parameters:

$$AIC = N\ln(\chi^2) + 2K \tag{18}$$

where χ is the fitting error (Eq. 16) presented in Fig. 1a, K is the number of the fitting parameters, N is the number of experimental parameters (relaxation times and dipolar order parameters) for each residue. The AIC has in this form been used in systems biology, e.g., for fitting of biochemical reaction rates using a similar fitting algorithm based upon stochastic searching (Abdullah et al. 2013), and we here tentatively apply it to our data, using the specific residual sum of squares, χ^2. It is assumed that the optimal fitting model is the one which has the minimal *AIC* value. The table of the *AIC*'s for all models and all residues can be found in the Supplementary material, Table S3. Thus, we may choose the optimal model for each residue. At the same time, we would not like to overestimate the significance of the model selection based on the *AIC*. Because of the noise of the experimental data, this selection is quite ambiguous. Future efforts are certainly necessary in order to further substantiate the way in which the *AIC* or a related criterion is to be applied to the fitting of a dataset with insufficient statistics and relatively low S/N ratio to the given formulae, evaluating parameter interdependencies, the influence of specific measurement errors, etc.

The minimal values of the *AIC* for the simplest "one component" model for certain residues do not mean that these residues undergo only one type of motion. This merely means that the data noise for these residues does not allow us to define unambiguously a more complicated form of the motional correlation function. On the other hand, it is evidently seen that there is an appreciable portion of residues for which the most complicated "three components" model appears to be the best description of the data according to the *AIC*. This demonstrates that the inclusion of the abundant $R_{1\rho}$ data in general requires more complicated fitting models than used in previous studies which we consider as one of the important results of the present work.

In addition to *AIC*'s presented in Table S3, we also calculated *AIC*'s based on the definition of χ normalized not to the experimental error of parameters (Eq. 16) but to the absolute values of these parameters:

$$\chi_{abs} = \sqrt{\frac{1}{N+1}\left(\sum_{i=1}^{N}\left(\frac{T^i_{\exp}-T^i_{sim}}{T^i_{\exp}}\right)^2 + \left(\frac{S^2_{\exp}-S^2_1\cdot S^2_2\cdot S^2_3}{S^2_{\exp}}\right)^2\right)} \tag{19}$$

We note that normalization (rather than using the simple sum of squares) is certainly necessary in a fit to experimental quantities covering very different value ranges (different relaxation times vs. order parameters), in order to not bias the fit and the *AIC* to the larger absolute differences when large numbers are fitted. The results are presented in Table S4. Since the minimization and *AIC* calculations were performed using different expressions, Eqs. (16) and (19), respectively, we expectedly observe an increase of the portion of residues that fit to the "one component" model: the number of fitting parameters is in this case more significant than the fitting error. In spite of this, there is an appreciable portion of residues for which the "three components" model is again identified as the most optimal model. Below, we refer to the *AIC*'s defined according to Eq. (16).

Table S3 shows that the "two components with distribution" model (χ) in comparison to other models provides an improved fitting quality only for very few residues. Thus, for the sake of unification and simplicity of the data presentation below, we will only discuss the results of the discrete models, since they enable simple and direct comparison of the dynamic parameters for different residues. For this, we have chosen the minimal *AIC* values only among three discrete models.

A set of fitting results for all models is shown in Figs. S2–S5 in the Supplementary material. These data are summarized in a more compact form in Fig. 3. It presents motional correlation times with a greyscale-coded discrimination by amplitude and motional amplitudes with a greyscale-coded discrimination by correlation time as a function of the residue number. The selection of the fitting model for each residue was performed using *AIC*'s among three discrete models as describe above. At the same time, we would like to stress again that the *AIC*-based validation of the different models should not be overestimated, the main conclusions of this work are drawn mainly from the analysis of all the presented models.

Motional amplitude as a function of time scale and sensitivity to low-amplitude motions

Figure 3a shows that all the motions we observe in the protein can be divided into three different time-scale domains: the fast motions with the correlation time shorter than 10^{-10} s, intermediate motions with the correlation times between $\sim 10^{-9}$ s and $\sim 2 \times 10^{-7}$ s and slow

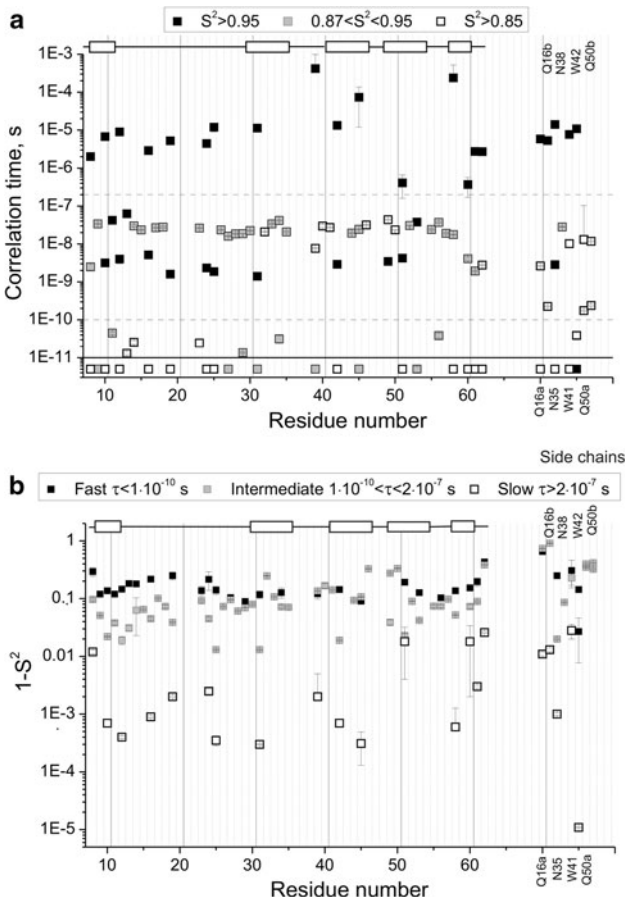

Fig. 3 **a** Correlation times (with order parameter encoded by the sign shading) and **b** motional amplitudes (with correlation time encoded by the sign shading) as a function of a residue number. The *solid line* in **a** depicts the limit of correlation times below which the value of the correlation time remains undefined. *Dashed lines* define the limits for the division for the fast, intermediate and slow motions

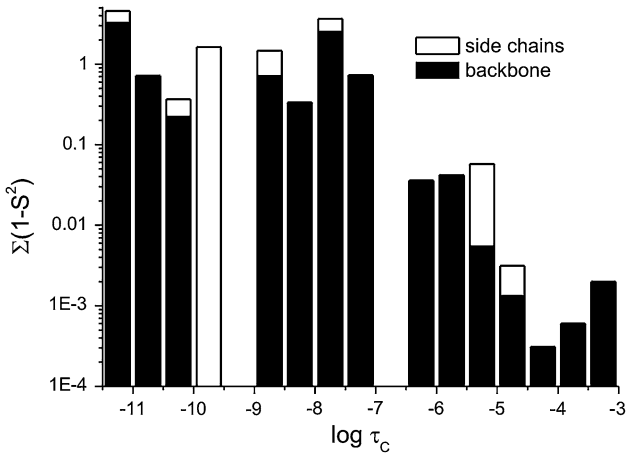

Fig. 4 Histogram of summarized amplitudes ($1 - S^2$) for all peaks as a function of the time scale of motion. The fitting models for each residue were chosen according to the *AIC* values

motions with correlation time longer $\sim 2 \times 10^{-7}$ s. The differentiation into these three categories is of course arbitrary; however we will use it in the following for the sake of discussion and interpretation. One may see that the slower the motion, the smaller amplitude it has. However, the decrease of the amplitude with increase of the correlation time is not monotonic. Figure 4 presents a histogram of the summed amplitudes of motions in the protein as a function of the correlation time. This histogram demonstrates quite interesting features of the backbone dynamics which has not been noticed so far.

All the mobility can be divided into three time-scale groups which obviously reflect the different natures of the motions on different time-scales. We see that there are two peaks with roughly similar intensities corresponding to the fast ($\tau < 10^{-10}$ s) and intermediate (10^{-9} s $< \tau < 10^{-7}$ s) motions separated by a gap of about one order of magnitude width. This motional "dead zone" of the backbone dynamics is quite a surprise. On the other hand, such a definite separation of two qualitatively different kinds of motions along the time scale axis looks quite reasonable. Fast motions are local oscillations of the N–H vector within steric hindrances and all slower motions are the correlated changes of the several degrees of the conformational freedom. On the slower time scale we see one more, although less pronounced, gap around 10^{-7} s and then a sharp decrease of the motional amplitude of about one order of magnitude. We would like to stress that the same diagrams plotted for the "two components", "three components" and "two components with distribution" models regardless the *AIC* values (Figs. S6–S8) qualitatively provide a very similar picture: fast and intermediate motions peaks separated by a gap and a sharp decrease of the motional amplitude within the timescale range 10^{-6}–10^{-7} s. Thus, the features we observe are model-independent. The fact that the amplitude of the slow motion of the protein backbone is much smaller than that of the fast motion has been noticed well before (Mack et al. 2000). However, our data clearly indicate that the tendency of decreasing amplitude with increasing time scale of the motion is pronouncedly non-monotonic, there are "ups" and "downs" on this dependence which is a result of the complex nature of the backbone mobility.

One of the most interesting results of the analysis is a detection of the slow motions in the microsecond time scale. In all cases the amplitude of these motions is very low, in some cases the order parameter has a value around 0.999. It may appear very surprising that such low amplitude motions can be experimentally detected at all, we however emphasize that this is a real result.

The data in Fig. 5 highlights that very low amplitudes of slow processes can indeed be reliably determined on the basis of $T_{1\rho}$ data. In this figure, experimental data are compared with two sets of calculated data assuming the

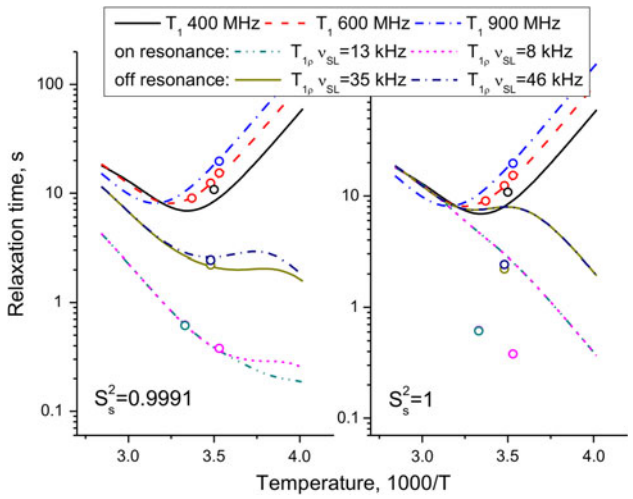

Fig. 5 Experimental (*circles*) and simulated (*curves*) relaxation times for the residue Q16. The *curves* were simulated according to the "three components" model and the parameters: $S_f^2 = 0.78$; $\tau_f < 10^{-11}$ s; $S_i^2 = 0.956$; $\tau_i = 5.1 \times 10^{-9}$ s; $\tau_s = 2.9 \times 10^{-6}$ s. $S_s^2 = 0.9991$ (*left*) and $S_s^2 = 1.0$ (*right*)

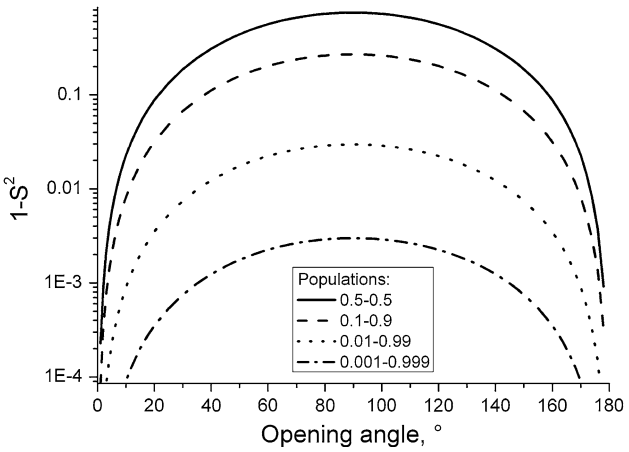

Fig. 6 Dependence of $1 - S^2$ on the opening angle for a "two-sites jumps" model for different relative site populations

order parameter of the microsecond motion to be 0.999 and exactly 1, respectively. Only in the former case the calculation can describe the $T_{1\rho}$ data, while the T_1's are expectedly not affected by the slow motion. This is a convincing demonstration of the advantage of using $T_{1\rho}$ experiments for studying slow internal protein dynamics. The explanation is in fact somewhat trivial, but is apparently not common knowledge. For cases where the frequency at which the spectral density function, Eq. (9), is evaluated is considerably smaller than the correlation time (i.e., $\omega\tau \ll 1$, fast motion limit), we have $J(\omega) \approx (1 - S^2)\tau$, which means that even when the amplitude $(1 - S^2)$ is low, the product $(1 - S^2)\tau$ and thus the spectral density that drives the relaxation may still be significant if only τ is long enough. This condition is easily fulfilled for low-frequency spin lock frequencies and motions in the µs range.

One may of course wonder about the significance of motional amplitudes in the (sub)percent range. Note again that by their physical nature, the slow motions are infrequent large-amplitude jumps between a small number of distinct conformational states (Henzler-Wildman and Kern 2007). At first sight, our data contradict this notion since the order parameter for the slow motions is very high. This apparent contradiction can be reasonably explained taking into account that the order parameter depends not only on the geometric amplitude of motion (jump angle), but also on the relative populations of different (conformational) sites. If the populations of these conformations (e.g., so-called ground vs. excited states/conformations) are very different, then the observed $(1 - S^2)$ would be very low even if the conformations are rather different. This is illustrated by the simulations of the order parameter (i.e., apparent motional amplitude) for two-site jumps with different populations of the sites, as plotted in Fig. 6. We are not aware of relevant studies of SH3 domain, but for some other proteins such slow conformational exchange processes between unequally populated sites can be observed using the liquid-state NMR methods based on chemical-exchange (R_2 or $R_{1\rho}$ dispersions) and residual dipolar coupling (RDC) measurements in orienting media (Korzhnev et al. 2004; Tolman and Ruan 2006; Markwick et al. 2007; Ban et al. 2011). In fact, such experiments even permit the extraction of the chemical shifts of the weakly populated excited state and to use them to determine their structure (Bouvignies et al. 2011). However, the liquid state methods can detect the excited states only if their population is not less that 0.5–1 %. The capabilities of the solid state approaches seem to be somewhat better: although the experimental accuracy of the solid state NMR relaxation methods is generally worse, the contribution from the low-amplitude slow motion involving an excited state to the relaxation rate is much larger than the experimental error, as demonstrated in Fig. 5.

Dynamics and secondary structure

It has been already reported that raw experimental parameters (relaxation times, dipolar couplings, etc.) have a certain correlation with a secondary structure of a protein (Chevelkov et al. 2008; Yang et al. 2009). This correlation is not very strict, it however indicates that the residues in the unstructured domains and on the ends of the secondary structure elements are more mobile than the residues within α-helices and β-sheets. Our analysis enables us to go further and to check the correlation between the secondary structure and internal dynamics in the different time-scale ranges. Table 1 presents the average amplitudes $(1 - S^2)$ and their RMS deviations of fast, intermediate and slow

Table 1 Mean and RMSD values of the motional amplitudes ($1 - S^2$) for different types of motions, experimental amplitudes from the dipolar order parameters, relaxation rates R_1 and $R_{1\rho}$ for β-sheets, unstructured domains and side chains

Time scale of the motion	β-sheets	Unstructured	Side chains
Motional amplitudes, model selection based on *AIC* values			
Fast	0.08 ± 0.084	0.144 ± 0.112	0.172 ± 0.231
Intermediate	0.109 ± 0.1	0.088 ± 0.076	0.399 ± 0.357
Slow	0.0017 ± 0.0055	0.0023 ± 0.0057	0.0067 ± 0.01
Motional amplitudes, "two components" model			
Fast	0.072 ± 0.056	0.092 ± 0.057	0.043 ± 0.079
Intermediate	0.111 ± 0.101	0.095 ± 0.056	0.388 ± 0.299
Slow	$4.3 \times 10^{-5} \pm 1.6 \times 10^{-4}$	0.01 ± 0.031	0.006 ± 0.008
Motional amplitudes, "three components" model			
Fast	0.147 ± 0.061	0.18 ± 0.07	0.308 ± 0.207
Intermediate	0.066 ± 0.072	0.059 ± 0.081	0.325 ± 0.324
Slow	0.0086 ± 0.018	0.0114 ± 0.027	0.0082 ± 0.0094
Experimental NMR parameters			
$1 - S^2$	0.203 ± 0.062	0.233 ± 0.112	0.4935 ± 0.308
R_1 @ 600 MHz, t = 14 °C	0.173 ± 0.129 s^{-1}	0.282 ± 0.425 s^{-1}	0.496 ± 0.476 s^{-1}
On-resonance $R_{1\rho}$ @spin-lock 8 kHz, t = 10 °C	5.04 ± 5.32 s^{-1}	4.63 ± 6.4 s^{-1}	7.06 ± 7.83 s^{-1}

motions for β-sheets (SH3 domain has no α-helices), unstructured domains, and side chains. This table presents the raw experimental data as well—dipolar order parameters, R_1 and $R_{1\rho}$ data. Our data demonstrate that fast motions have on average smaller amplitude in β-sheets which corresponds to the previous data. On the other hand, taking into account the RMSD's one can hardly say that this correlation is well defined and significant. As for the intermediate and slow motions, our data, both fitting results and raw experimental parameters, show no correlation at all. As for the side chains, they simply appear to be more mobile on all time scales.

Studying slow motions: fitting solid state NMR data versus comparison of the liquid and solid-state order parameters

An approach to studying slow (ns-μs time scale) dynamics in SH3 domain was attempted via a comparison of liquid- and solid-state ^{1}H-^{15}N motionally averaged dipolar couplings (Chevelkov et al. 2010). Liquid-state order parameters obtained from a Lipari-Szabo analysis of the relaxation times (S^2_{rel}) correspond to the internal motions faster than the overall tumbling, which is about 5 ns for SH3 at ambient temperature, whereas dipolar couplings measured in the solid state (S^2_{DC}) are a measure of the integral amplitude of all motions with correlation times faster than ~1 μs. Thus, the experimentally observed differences between S^2_{rel} and S^2_{DC} are indicative of internal motions on a time scale of about ~5 ns to ~1 μs, respectively. Such a difference was observed only for two residues, L8 and T24, while all others reveal approximately the same liquid- and solid-state order parameters. From this one may be tempted to conclude that the protein undergoes practically no slow motions. To compare the results of this work with our analysis, Fig. 7 shows the product $S^2_{\text{int}} \cdot S^2_{\text{slow}}$ (if the correlation time of the intermediate motion is shorter than 5 ns, we assume S^2_{int} to be equal to 1) as a function of residue number. From this figure it is clear that: (1) significant portion of the residues undergo motions in the slow time scale with an appreciable amplitude and (2) residues 8 and 24 do not show any specific features in comparison with their neighbors. There are two reasons that can explain the discrepancy between the results of the present work and (Chevelkov et al. 2010). First, the amplitude of the slow motion for most residues is rather low as compared to the overall accuracy of the order parameters determination: note that in some cases $S^2_{\text{rel}} < S^2_{\text{DC}}$ (Chevelkov et al. 2010) which is unphysical and can only be explained by experimental errors. Second, S^2_{rel} was calculated from the relaxation times assuming the simplest Lipari-Szabo model with only one mode of internal motion which is likely an oversimplification.

In this context we mention two more examples of comparisons of liquid- and solid-state order parameters. The first one is thioredoxin, (Yang et al. 2009) where statistically the solid-state order parameters were found to be a bit lower than the liquid-state ones, but in most cases the difference is on the level of the accuracy of the measurements. The second example is ubiquitin. Fig. S9 compares the order parameters determined from the liquid state NMR relaxation times (Chang and Tjandra 2005), from RDC in oriented media experiments (Salmon et al. 2009) and solid-state NMR experiments (Schanda 2013) (the solid-state order parameters presented in Fig. S9 in Supplementary material

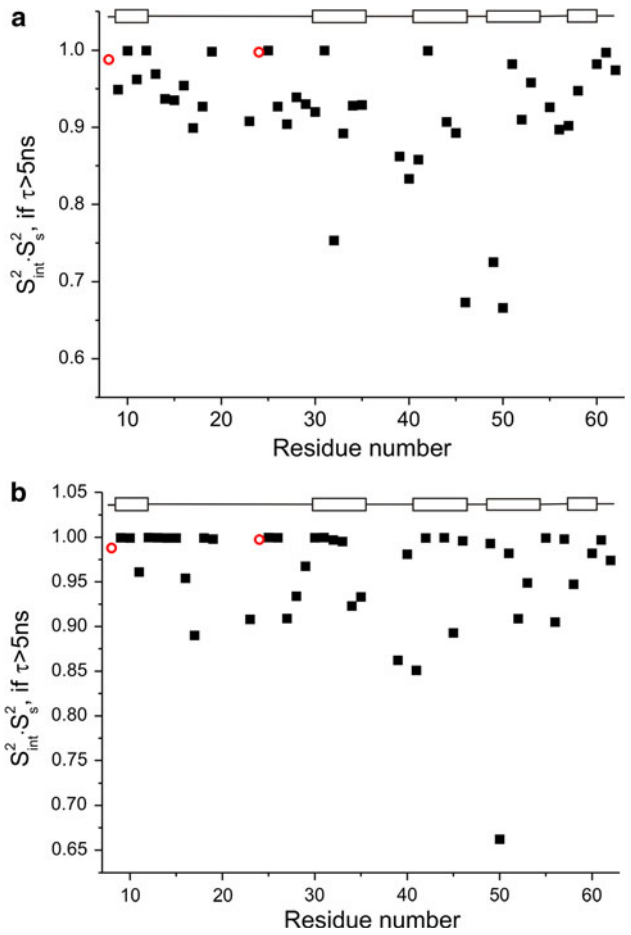

Fig. 7 Product of the order parameters of motions slower than the overall tumbling of the SH3 domain in solution. Fitting models: *AIC* values (**a**) and "three components" model (**b**). Residues L8 and T24 are marked as *red open circles*

differ from the ones published previously by the same authors for the same protein (Schanda et al. 2010); the more recent data should be considered as more correct). The three sets of data reveal a rather weak statistically relevant difference and, as in the case of SH3 domain, the experimental error is rather significant, as is indicated by a large number of residues for which $S^2_{rel} < S^2_{DC}$ and S^2_{rel}, $S^2_{DC} < S^2_{RDC}$. From these examples we conclude that the comparison of the liquid- and solid-state order parameters can hardly provide reliable information on the internal mobility on the ns-μs time scale range. On the other hand, our analysis with emphasis on $R_{1\rho}$ demonstrates that almost all residues undergo motions in this time scale, although these motions have rather low apparent amplitudes, as they likely relate to weakly populated states.

Relaxation rates and dynamic parameter correlations

Previously we have noticed that the R_1 and $R_{1\rho}$ profiles in SH3 domain appear to be quite similar (Krushelnitsky et al. 2010), and the same trend can be seen in the R_1 and $R_{1\rho}$ data in GB1 protein (Lewandowski et al. 2011). On the basis of this observation we hypothesized that the internal protein motions in the nanosecond and microsecond time scales maybe correlated: the protein domains undergoing significant fast motions also reveal increased-amplitude slow motions. The data obtained in the present study allow us to scrutinize this hypothesis. We tried to find correlations between various dynamic parameters obtained from the fitting but failed revealing any clear correlation between any pair of order parameters or correlation times, at least within the accuracy of the currently available data. Thus, the hypothesis turns out to be incorrect. Internal motions on different time scales are not correlated, at least not locally on the level of one and the same residue.

The observed R_1–$R_{1\rho}$ correlation in fact can be explained by the amplitude of the intermediate motion, as shown in Fig. 8, where this quantity is correlated with either of the two relaxation rates. Intermediate motions contribute equally both to R_1 and $R_{1\rho}$ rates since their correlation time ranges between ns and μs. Thus, a variation of the intermediate motion amplitude along the polypeptide chain causes variations of both R_1 and $R_{1\rho}$ rates, which explains the observed R_1–$R_{1\rho}$ correlation. In addition to that, we tried to find correlations between the dynamic parameters obtained in the present study and the parameters of the ms-s motions observed by the dipolar CODEX experiments (Krushelnitsky et al. 2009) but also failed.

The conclusion on the absence of any correlation between mobility on different time scales seems to contradict the conclusion of Yang et al. (Yang et al. 2009), who measured and compared several types of NMR data (R_1's, liquid-state order parameters, motionally averaged solid-state dipolar couplings and CSA tensors) in thioredoxin. All the data appeared to be correlated, from which the authors concluded that fast librations on the sub-ns time scale (reflected in R_1's and liquid-state order parameters) modulate slower motions (reflected in dipolar couplings and CSA tensors). The observed correlations can, however, be explained in a more simple way. All these NMR parameters are in a large extent determined by the amplitude of the fast motion. Since the amplitude of the fast motions is larger or at least similar in comparison to that of the slower motions, as shown herein, fast motions have a significant impact on the values of all these parameters. Thus, these parameters may seem to be correlated (because of the fast motion only) even if fast and slow motions are not correlated at all. We thus do not believe that these correlations indicate any clear connection between internal dynamics on different time scales. This conclusion corresponds to the results of our recent comparison of solid-state NMR data and B-factors derived from X-ray crystallographic data for the same proteins (Reichert et al. 2012).

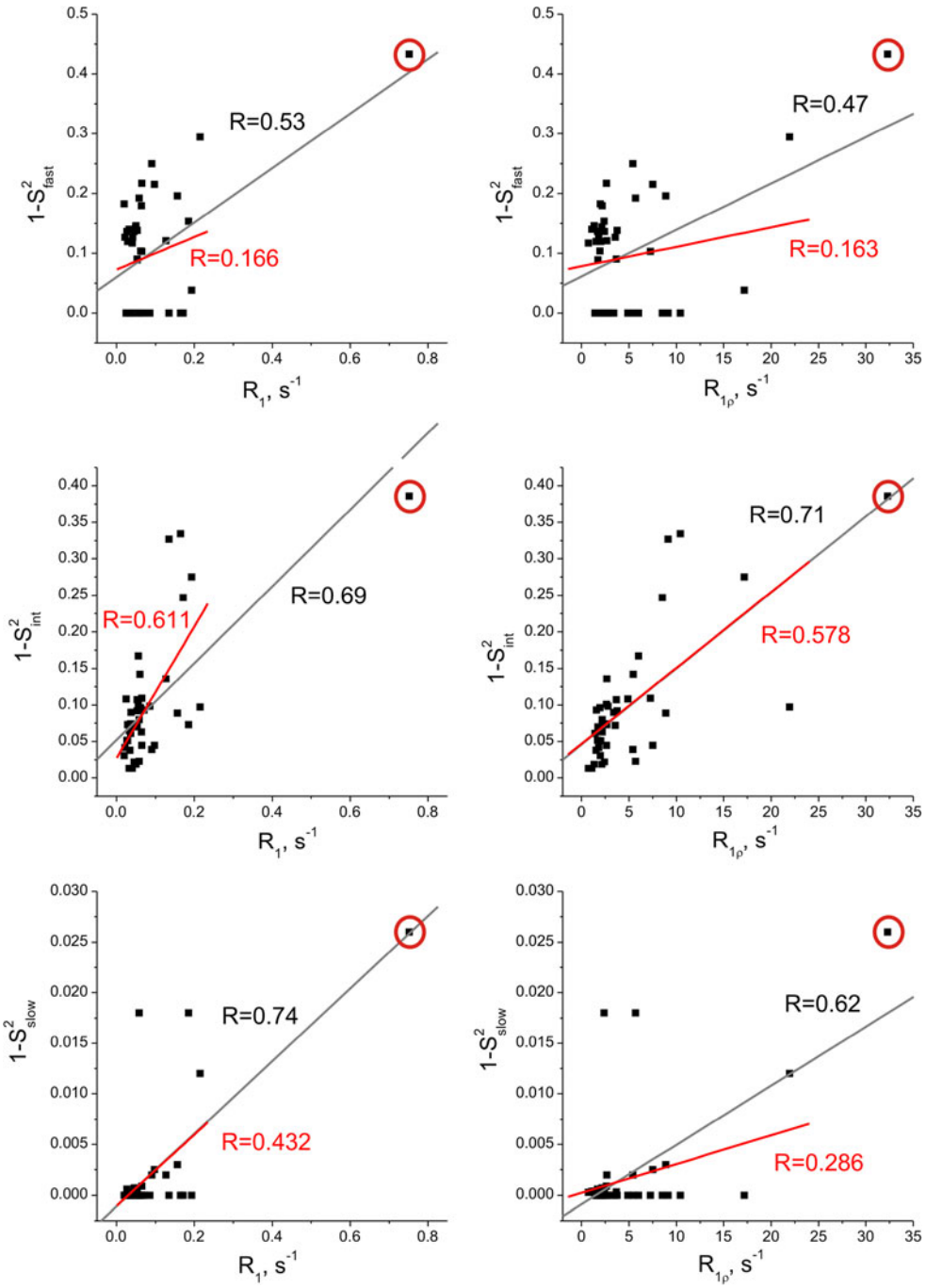

Fig. 8 $R_{1\rho}/R_1$—motional amplitudes $(1 - S^2)$ correlation plots for the fast (*top*), intermediate (*middle*) and slow (*bottom*) motions. The model selection for each residue was based on the *AIC* values. The residue D62 which has abnormally high relaxation rates is marked by a *red circle*. The correlation coefficients are calculated with (*black*) and without (*red*) D62 data. It is seen that the significant level of the correlation remains after taking off the D62 rates only for the intermediate motion. R_1's were measured at 600 MHz and t = 12 °C; $R_{1\rho}$'s were measured at 400 MHz, on-resonance spin-lock frequency 8 kHz, MAS 20 kHz and t = 10 °C

Both NMR parameters and B-factors are indicators of internal motions, thus one may expect that these data can be somehow correlated. However, we have demonstrated that in general, except trivial cases of unstructured domains, there is no correlation between X-ray and NMR parameters, supporting our argument.

Conclusions

The analysis of an abundant set of NMR data enabled a step forward in understanding the nature of internal conformational dynamics of proteins, and in particular, a critical review of a number of hypotheses from the current

literature. The inclusion of relaxation times $T_{1\rho}$ measured at different spin-lock fields, MAS and offset frequencies has revealed that the two-component correlation function that has previously been used in fitting the solid-state NMR data in proteins is satisfactory only for a certain fraction of the residues. There are, however, many examples for which a more complex model of the correlation function and a larger number of fitting parameters are necessary.

The analyses demonstrated that the slowest motions that can be detected by means of the relaxation methods have a correlation time around 10^{-6}–10^{-5} s. Up to now such slow dynamics was mainly studied by means of liquid-state chemical-exchange and RDC-based methods. Solid-state NMR methods seem to be somewhat more sensitive to exchange between sites with a very different lifetime (leading to different equilibrium populations) than the liquid-state approaches. At the same time, we admit that the typical experimental error of solid-state NMR relaxation times is still too high for an unambiguous choice between various fitting models since quite often different models provide practically the same fitting quality. The precision of the analysis can be significantly improved by more accurate measuring the slopes of the temperature dependences (apparent activation energies) of the relaxation rates even within a narrow range of temperatures. These slopes are much more informative for the determination of the correlation times than the absolute values of the rates themselves. The price to pay is of course an increased number of experiments, which is not always feasible or even affordable.

On the basis of our data, we checked correlations between secondary structure and the dynamics, and between motions and their amplitudes on different time scales. Our results do not contradict to previous findings which indicated that within the secondary structure elements internal dynamics is somewhat suppressed. However, we found that this holds only for fast ($\tau < 10^{-9}$ s) motions, while for the slower motions, no correlation with the secondary structure is apparent. As to comparing mobility on different time scales, one general tendency is rather apparent: the slower the motion, the higher its order parameter, thus, the lower its apparent amplitude. This tendency is, however, not monotonic—the data indicates that there is a gap in the 10^{-10}–10^{-9} s range separating fast and slow motions with different physical nature, i.e., possibly, collective librations and large-angle jumps between rather unevenly populated sites, respectively. As to residue-by-residue comparisons between motions on different time scales, our data do not support any significant correlation. It is often assumed that fast motions play a role of precursor of the slower motions and hence, the residues undergoing increased mobility in the faster time scale may also reveal increased-amplitude slower motions. This assumption however is not confirmed by our data, at least on the level of a single residue, suggesting the importance of cooperative dynamics and inter-residue contacts. The nature of protein conformational dynamics is often too complicated to be described by simple models and notions.

Electronic supplementary material

Table of all the experimental relaxation times and dipolar order parameters along with the simulated values; simulated correlation functions for the wobbling in a cone model along with the fitting curves using Fuoss-Kirkwood distribution function; table of the activation energy limits during the Monte-Carlo minimization for all four fitting models; fitting results for all four fitting models; table of χ and *AIC* values for all residues and models; amplitude—time scale histogram for the "two components" and "three components" models; comparison of the liquid state and solid state order parameters for ubiquitin.

Acknowledgments We thank the Deutsche Forschungsgemeinschaft (DFG, SFB-TRR 102 project A8) for funding this work. Fruitful discussions with Dr. Paul Schanda and Prof. Christian Griesinger are greatly acknowledged.

References

Abdullah A, Deris S, Anwar S, Arjunan SNV (2013) An evolutionary firefly algorithm for the estimation of nonlinear biological model parameters. PLoS ONE 8:e56310

Agarwal V, Xue Y, Reif B, Skrynnikov NR (2008) Protein side-chain dynamics as observed by solution- and solid-state NMR spectroscopy: a similarity revealed. J Am Chem Soc 130: 16611–16621

Akaike H (1974) Stochastic theory of minimal realization. IEEE Trans Automat Contr 19:667–674

Akasaka K (1983) Spin–spin and spin-lattice contributions to the rotating frame relaxation of ^{13}C in L-alanine. J Chem Phys 78:3567–3572

Baldus M (2002) Correlation experiments for assignment and structure elucidation of immobilized polypeptides under magic angle spinning. Prog Nucl Magn Reson Spectrosc 41:1–47

Ban D, Funk M, Gulich R, Egger D, Sabo TM, Walter KFA, Fenwick RB, Giller K, Pichierri F, de Groot BL, Lange OF, Grubmüller H, Salvatella X, Wolf M, Loidl A, Kree R, Becker S, Lakomek N-A, Lee D, Lunkenheimer P, Griesinger C (2011) Kinetics of conformational sampling in ubiquitin. Angew Chem 123: 11639–11642

Beckmann P (1988) Spectral densities and nuclear spin relaxation in solids. Phys Rep 171:85–128

Bertini I, Emsley L, Felli IC, Laage S, Lesage A, Lewandowski JR, Marchetti A, Pieratelli R, Pintacuda G (2011) High-resolution and sensitivity through-bond correlations in ultra-fast magic angle spinning (MAS) solid-state NMR. Chem Sci 2:345–348

Böckmann A (2008) 3D protein structures by solid-state NMR spectroscopy: ready for high resolution. Angew Chem Int Ed 47:6110–6113

Bouvignies G, Vallurupalli P, Hansen DF, Correia BE, Lange O, Bah A, Vernon RM, Dahlquist FW, Baker D, Kay LE (2011) Solution structure of a minor and transiently formed state of a T4 lysozyme mutant. Nature 477:111–114

Castellani F, Van Rossum B, Diehl A (2002) Structure of a protein determined by solid-state magic-angle-spinning NMR spectroscopy. Nature 420:98–102

Chang S-L, Tjandra N (2005) Temperature dependence of protein backbone motion from carbonyl ^{13}C and amide ^{15}N NMR relaxation. J Magn Reson 174:43–53

Chekmenev EY, Zhang Q, Waddell KW, Mashuta MS, Wittebrot RJ (2004) ^{15}N Chemical shielding in glycyl tripeptides: measurement by solid-state NMR and correlation with X-ray structure. J Am Chem Soc 126:379–384

Chevelkov V, Rehbein K, Diehl A, Reif B (2006) Ultrahigh resolution in proton solid-state NMR spectroscopy at high levels of deuteration. Angew Chem Int Ed 45:3878–3881

Chevelkov V, Zhuravleva AV, Xue Y, Reif B, Skrynnikov NR (2007) Combined analysis of ^{15}N relaxation data from solid- and solution-state NMR Spectroscopy. J Am Chem Soc 129: 12594–12595

Chevelkov V, Diehl A, Reif B (2008) Measurement of ^{15}N-T1 relaxation rates in a perdeuterated protein by magic angle spinning solid-state nuclear magnetic resonance spectroscopy. J Chem Phys 128:052316

Chevelkov V, Fink U, Reif B (2009a) Accurate determination of order parameters from ^{1}H,^{15}N dipolar couplings in MAS solid-state NMR experiments. J Am Chem Soc 131:14018–14022

Chevelkov V, Fink U, Reif B (2009b) Quantitative analysis of backbone motion in proteins using MAS solid-state NMR spectroscopy. J Biomol NMR 45:197–206

Chevelkov V, Xue Y, Linser R, Skrynnikov NR, Reif B (2010) Comparison of solid-state dipolar couplings and solution relaxation data. J Am Chem Soc 132:5015–5017

Clore GM, Szabo A, Bax A, Kay LE, Driscoll PC, Gronenborn AM (1990) Deviations from the simple two-parameter model-free approach to the interpretation of nitrogen-15 nuclear magnetic relaxation of proteins. J Am Chem Soc 112:4989–4991

Cole HBR, Torchia DA (1991) An NMR study of the backbone dynamics of staphylococcal nuclease in the crystalline state. Chem Phys 158:271–281

Daragan V, Mayo K (1997) Motional model analyses of protein and peptide dynamics using ^{13}C and ^{15}N NMR relaxation. Prog Nucl Magn Reson Spectrosc 31:63–105

Dayie KT, Wagner G, Lefèvre JF (1996) Theory and practice of nuclear spin relaxation in proteins. Annu Rev Phys Chem 47:243–282

Doi M, Edwards SF (1986) The theory of polymer dynamics. Clarendon Press, Oxford

Fedotov V, Schneider H (1989) Structure and dynamics of bulk polymers by NMR methods. Springer, Berlin

Ferry JD (1980) Viscoelastic properties of polymers. Wiley, New York

Franks WT, Zhou DH, Wylie BJ, Money BG, Graesser DT, Frericks HL, Sahota G, Rienstra CM (2005) Magic-angle spinning solid-state NMR spectroscopy of the beta1 immunoglobulin binding domain of protein G (GB1): ^{15}N and ^{13}C chemical shift assignments and conformational analysis. J Am Chem Soc 127:12291–12305

Gaspari Z, Perczel A (2010) Protein dynamics as reported by NMR. Annu Rep NMR Spectrosc 71:35–75

Giraud N, Blackledge M, Goldman M, Böckmann A, Lesage A, Penin F, Emsley L (2005) Quantitative analysis of backbone dynamics in a crystalline protein from nitrogen-15 spin-lattice relaxation. J Am Chem Soc 127:18190–18201

Hackel C, Zinkevich T, Belton P, Achilles A, Reichert D, Krushelnitsky A (2012) The trehalose coating effect on the internal protein dynamics. Phys Chem Chem Phys 14:2727–2734

Haliloglu T, Bahar I, Erman B (1997) Gaussian dynamics of folded proteins. Phys Rev Lett 79:3090–3093

Hall JB, Fushman D (2006) Variability of the ^{15}N chemical shielding tensors in the B3 domain of protein G from ^{15}N relaxation measurements at several fields. Implications for backbone order parameters. J Am Chem Soc 128:7855–7870

Henzler-Wildman K, Kern D (2007) Dynamic personalities of proteins. Nature 450:964–972

Herzfeld J, Roberts JE, Griffin RG (1987) Sideband intensities in two-dimensional NMR spectra of rotating solids. J Chem Phys 86:597

Johnson E, Palmer A, Rance M (2007) Temperature dependence of the NMR generalized order parameter. Protein Struct Funct Bioinf 66:796–803

Kleckner IR, Foster MP (2011) An introduction to NMR-based approaches for measuring protein dynamics. Biochim Biophys Acta 1814:942–968

Korzhnev DM, Billeter M, Arseniev AS, Orekhov VY (2001) NMR studies of Brownian tumbling and internal motions in proteins. Prog Nucl Magn Reson Spectrosc 38:197–266

Korzhnev D, Salvatella X, Vendruscolo M, Di Nardo AA, Davidson AR, Dobson SM, Kay LE (2004) Low-populated folding intermediates of Fyn SH3 characterized by relaxation dispersion NMR. Nature 430:586–590

Kremer F, Schonhals A (2003) Broadband dielectric spectroscopy. Springer, Berlin

Kroenke C, Loria J, Lee L (1998) Longitudinal and transverse ^{1}H-^{15}N dipolar/^{15}N chemical shift anisotropy relaxation interference: unambiguous determination of rotational diffusion tensors and chemical exchange effects in biological macromolecules. J Am Chem Soc 120:7905–7915

Krushelnitsky A, Kurbanov R, Reichert D, Hempel G, Schneider H, Fedotov V (2002) Expanding the frequency range of the solid-state T1rho experiment for heteronuclear dipolar relaxation. Solid State Nucl Magn Reson 22:423–438

Krushelnitsky A, DeAzevedo E, Linser R, Reif B, Saalwächter K, Reichert D (2009) Direct observation of millisecond to second motions in proteins by dipolar CODEX NMR spectroscopy. J Am Chem Soc 131:12097–12099

Krushelnitsky A, Zinkevich T, Reichert D, Chevelkov V, Reif B (2010) Microsecond time scale mobility in a solid protein as studied by the ^{15}N R(1rho) site-specific NMR relaxation rates. J Am Chem Soc 132:11850–11853

Kurbanov R, Zinkevich T, Krushelnitsky A (2011) The nuclear magnetic resonance relaxation data analysis in solids: general R1/R1(ρ) equations and the model-free approach. J Chem Phys 135:184104

Lewandowski JR, Sein J, Sass HJ, Grzesiek S, Blackledge M, Umsley L (2010) Measurement of site-specific ^{13}C spin-lattice relaxation in a crystalline protein. J Am Chem Soc 132:8252–8254

Lewandowski JR, Sass HJ, Grzesiek S, Blackledge M, Emsley L (2011) Site-specific measurement of slow motions in proteins. J Am Chem Soc 133:16762–16765

Lipari G, Szabo A (1982a) Model-free approach to the interpretation of nuclear magnetic resonance relaxation in macromolecules. 2. Analysis of experimental results. J Am Chem Soc 104: 4559–4570

Lipari G, Szabo A (1982b) Model-free approach to the interpretation of nuclear magnetic resonance relaxation in macromolecules. 1. Theory and range of validity. J Am Chem Soc 104:4546–4559

Mack JW, Usha MG, Long J, Griffin RG, Wittebrot RJ (2000) Backbone motions in crystalline protein from field-dependent

2H-NMR relaxation and line-shape analysis. Biopolymers 53:9–18

Marchetti A, Jehle S, Felletti M, Knight MJ, Wang Y, Xu Z-Q, Par AY, Otting G, Lesage A, Emsley L, Dixon NE, Pintacuda G (2012) Backbone assignment of fully protonated solid proteins by ^{1}H detection and ultrafast magic-angle-spinning NMR spectroscopy. Angew Chem Int Ed 51:10756–10759

Markwick PRL, Bouvignies G, Blackledge M (2007) Exploring multiple timescale motions in protein GB3 using accelerated molecular dynamics and NMR spectroscopy. J Am Chem Soc 129:4724–4730

Marulanda D, Tasayco ML, Cataldi M, Arriaran V, Polenova T (2005) Resonance assignments and secondary structure analysis of *E. coli* thioredoxin by magic angle spinning solid-state NMR spectroscopy. J Phys Chem B 109:18135–18145

McCrum NG, Read BE, Williams G (1967) Anelastic and dielectric effects in polymeric solids. Wiley, London

Mollica L, Baias M, Lewandowski JR, Wylie BJ, Sperling LJ, Rienstra SM, Emsley L, Blackledge M (2012) Atomic resolution structural dynamics in crystalline proteins from molecular simulation and NMR. J Phys Chem Lett 3:3657–3662

Morin S (2011) A practical guide to protein dynamics from ^{15}N spin relaxation in solution. Prog Nucl Magn Reson Spectrosc 59: 245–262

Palmer A (2001) NMR probes of molecular dynamics: overview and comparison with other techniques. Annu Rev Biophys Biomol Struct 30:129–155

Reichert D, Zinkevich T, Saalwächter K, Krushelnitsky A (2012) The relation of the X-ray B-factor to protein dynamics: insights from recent dynamic solid-state NMR data. J Biomol Struct Dyn 30:617–627

Salmon L, Bouvignies G, Markwick P, Lakomek N, Showalter S, Li D-W, Walter K, Griesinger C, Brüschweiler R, Blackledge M (2009) Protein conformational flexibility from structure-free analysis of NMR dipolar couplings: quantitative and absolute determination of backbone motion in ubiquitin. Angew Chem Int Ed 48:4154–4157

Schanda P (2013) Personal communication, to be published

Schanda P, Meier BH, Ernst M (2010) Quantitative analysis of protein backbone dynamics in microcrystalline ubiquitin by solid-state NMR spectroscopy. J Am Chem Soc 132:15957–15967

Schanda P, Huber M, Boisbouvier J, Meier BH, Ernst M (2011) Solid-state NMR measurements of asymmetric dipolar couplings provide insight into protein side-chain motion. Angew Chem Int Ed 50:11005–11009

Tolman JR, Ruan K (2006) NMR residual dipolar couplings as probes of biomolecular dynamics. Chem Rev 106:1720–1736

VanderHart DL, Garroway AN (1979) ^{13}C NMR rotating frame relaxation in a solid with strongly coupled protons: polyethylene. J Chem Phys 71:2773–2787

Wylie BJ, Franks WT, Rienstra CM (2006) Determinations of ^{15}N chemical shift anisotropy magnitudes in a uniformly ^{15}N,^{13}C-labeled microcrystalline protein by three-dimensional magic-angle spinning nuclear magnetic resonance spectroscopy. J Phys Chem B 110:10926–10936

Wylie BJ, Sperling LJ, Frericks HL, Shah GJ, Franks WT, Riensta CM (2007) Chemical-shift anisotropy measurements of amide and carbonyl resonances in a microcrystalline protein with slow magic-angle spinning NMR spectroscopy. J Am Chem Soc 129:5318–5319

Yang J, Tasayco ML, Polenova T (2009) Dynamics of reassembled thioredoxin studied by magic angle spinning NMR: snapshots from different time scales. J Am Chem Soc 131:13690–13702

Yao L, Vögeli B, Ying J, Bax A (2008) NMR determination of amide N-H equilibrium bond length from concerted dipolar coupling measurements. J Am Chem Soc 130:16518–16520

Zech SG, Wand JA, McDermott AE (2005) Protein structure determination by high-resolution solid-state NMR spectroscopy: application to microcrystalline ubiquitin. J Am Chem Soc 127:8618–8626